Optically-induced defect states in photonic lattices: formation of defect channels, directional couplers, and disordered lattices leading to Anderson-like light localization

A. Kanshu · C.E. Rüter · D. Kip · V.M. Shandarov

Abstract Formation of defect states by optical induction in one-dimensional photonic lattices fabricated in photorefractive lithium niobate is investigated experimentally. First, by using a moving narrow laser beam for defect recording, we investigate light propagation in samples containing single line defects and adjacent channel defects forming directional couplers. Then, these results are used to create lattices with randomly distributed defects, resembling a disordered optical potential. In such lattices, wave propagation is found to change from ballistic transport to transverse Anderson-like light localization as a function of induced disorder.

PACS 42.65.Tg · 63.20.Pw · 42.25.Gy

1 Introduction

Wave propagation in periodic optical lattices (photonic crystals) has been intensively studied in the last years, including both theoretical and experimental investigations [1, 2]. Waveguide arrays (WA) are one- or two-dimensional (1D or 2D) realizations of such photonic lattices [3–5]. The linear solutions of a WA are extended Floquet–Bloch modes, which form a transmission spectrum (band structure) consisting of allowed bands, separated by forbidden gaps [6, 7]. Already in the linear case, wave propagation in such media

may be fundamentally different than in homogeneous ones [8, 9]. However, when such a periodic medium also possesses a nonlinearity, propagation dynamics can be strongly modified [10–13]. In the case of a narrow input beam, which locally alters the refractive index of the material, this beam may induce a defect state in the lattice and may be self-trapped by its own defect. In this way, a localized mode of the lattice is excited, and the formed nonlinear excitation is called a discrete soliton or lattice soliton, whose propagation constant is located inside the gap of the (linear) band structure [7, 10, 14, 15].

The introduction of zero-dimensional (point-like) or one-dimensional (line) defects into photonic crystals or WA offers various potential applications, like high-quality waveguide structures, optical routers, or laser cavities [16, 17]. Beside the possibility of induction of defect structures in a WA by the excited light beam itself, i.e., formation of lattice solitons, also (external) control beams can be used for defect formation [18, 19]. Such structures may be used to linearly guide or deflect other light beams [20, 21], or to form more complex integrated circuits like beam splitters and routers. In this work, we investigate experimentally the formation and light guiding/trapping properties of light-induced defects in a 1D WA. Single line defects, double adjacent defects, and extended disordered lattices are fabricated by direct laser beam recording using a nonlinear lithium niobate (LiNbO$_3$) substrate. In the following section, the experimental methods used to record single and multiple defects are described. Then, the first part of Sect. 3 is devoted to recording of single and double defects, and investigation of the guiding properties of the induced structures. Based on these initial results, in the second part of that section the formerly obtained results are used to form samples with randomly distributed defects among the whole array. In such disordered lattices, the effect of Anderson-like

A. Kanshu · C.E. Rüter · D. Kip (✉)
Institute of Energy Research and Physical Technologies, Clausthal University of Technology, 38678 Clausthal-Zellerfeld, Germany
e-mail: d.kip@pe.tu-clausthal.de

V.M. Shandarov
State University of Control Systems and Radioelectronics, 40 Lenin Ave., 634050 Tomsk, Russia

localization of light is investigated for WA with different disorder strength. Finally, a summary concludes the article.

2 Fundamentals and experimental methods

Light propagation in a 1D quasi-periodic WA may be well described by the paraxial time-independent Helmholtz equation. The propagation of the light electric field E along the z-direction in a lattice that is modulated and additionally locally distorted or disordered along the transverse x direction, thus follows [5]

$$i\frac{\partial E}{\partial z} + \frac{1}{2k_0 n_0}\frac{\partial^2 E}{\partial x^2} + k_0 n_0 n(x)E = 0, \qquad (1)$$

where $k_0 = 2\pi/\lambda$ is the wave number, n_0 is the refractive index of the substrate, and $n(x) = \Delta n(x) + \delta n(x)$ is a stationary transverse potential, containing both the regular periodic modulation $\Delta n(x)$ defining the lattice, and additional defects and/or disorder described by the function $\delta n(x)$.

Our nonlinear 1D WA is fabricated using an undoped LiNbO$_3$ substrate [5, 22]. The sample dimensions are $1 \times 20 \times 7.8$ mm^3 with the ferroelectric c-axis pointing along the 7.8 mm long x-axis. To increase the photovoltaic photorefractive nonlinearity the substrate is first covered with an 8.6 nm-thick Fe layer by e-beam evaporation. This layer is in-diffused in air at a temperature of 1273 K for a total diffusion time of 22 hours, resulting in an almost constant Fe concentration of about 0.05 wt.% over the waveguide region. In a second step, an array of parallel aligned channel waveguides is fabricated by patterning a 10 nm-thick Ti layer formed by sputtering on the same sample surface, using standard photolithographic techniques. In-diffusion of the Ti stripes takes place for 2 hours at a temperature of 1273 K in wet argon atmosphere. The final array consists of 250 channels with a width of 4.0 μm and separated by 3.6 μm (grating period $\Lambda = 7.6$ μm) aligned parallel to the 20 mm-long z-axis, which is the light propagation direction. The input and output facets (with dimensions of 1×7.8 mm^2) are optically polished to allow for coupling of light into and out of the WA. After this step the final propagation length of the sample is $L = 17.5$ mm.

The experimental scheme used to record single discrete or randomly distributed defects into a 1D WA is given in Fig. 1. Light of a frequency-doubled Nd:YVO$_4$ laser with wavelength $\lambda = 532$ nm is focused on the top surface of the LiNbO$_3$ WA using a $40\times$ microscope objective (NA = 0.65). The sample is mounted on a motorized xz-stage (Newport XMS). With the help of a CCD camera that monitors the back reflected light the diameter of the incident Gaussian beam is adjusted to be $w_0 = 4$ μm (FWHM, measured on the sample surface), which fairly well coincides with the width of a single channel of the WA, see
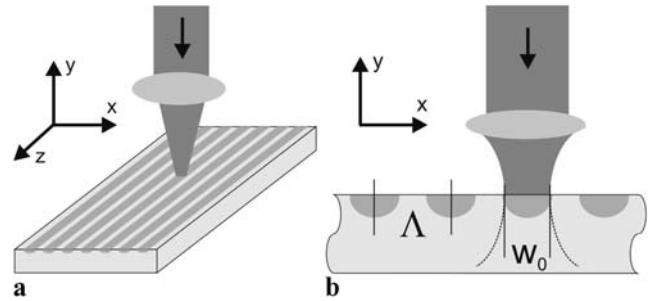
Fig. 1 Experimental scheme to form light-induced defect states in a 1D WA. (**a**) *Top view*: For each single defect (fixed x-coordinate) a focused light beam (wavelength $\lambda = 532$ nm) is scanned along the z-direction with constant velocity. (**b**) The beam diameter of the recording beam is adjusted to match the width of the in-diffused channel waveguide

Fig. 1(b). By using the same camera system the sample orientation can be precisely aligned to ensure parallel motion of the focused light spot along the waveguide channel direction. The recording light polarization is chosen to be extraordinary, i.e., parallel to the ferroelectric c-axis (x-direction) of the substrate. To record defect structures the optical power of the focused beam can be varied in a range $P = (0–44)$ mW. Local energy deposition depends on the scan velocity along the z-direction, which can be varied in a range $v = (4–80)$ μm/s. The maximum deposited local energy per unit area is thus $\tilde{E}_{max} = I \cdot \Delta t = P_{max}/(\pi w_0^2) \cdot w_0/v_{min} \approx 9 \times 10^8$ J/m^2, where P_{max} and v_{min} are maximum recording light power and minimum scan velocity, respectively. For this maximum deposited energy we may assume that the induced refractive index changes are already in saturation [23]. To test the guiding properties of defect structures we use another (low-power) laser source of the same wavelength and a standard coupling setup [5].

3 Results and discussion

3.1 Formation of single defect channels

To start with, we chose the most simple light-induced defect structure that can be formed in our sample, i.e., a single defect aligned on top of a certain waveguide channel. In future applications, such straight (or slightly curved) defect channels may form the basic "wires" for light in a two- or three-dimensional photonic crystal [16]. Such defects consist of a deviation of the otherwise regular periodic structure, i.e., an either increased or decreased refractive index when compared with the surrounding periodic medium. The corresponding propagation constants associated with these defects form isolated states located inside one of the gaps of the band structure. In a 1D WA, a positive defect (a single channel waveguide with increased refractive index) represents a defect state with increased index or propagation

constant, respectively, located above the first band in the total internal reflection semi-infinite gap. On the other hand, if the index of a single waveguide channel is decreased, a defect state in the first finite gap between bands one and two of the structure is formed [5].

In our experiments, we chose the latter type to record single-channel defects related to the negative photovoltaic nonlinearity of $LiNbO_3$. A focused Gaussian beam is scanned on-channel along z, while the x-position is adjusted to overlap with the index profile of a selected channel
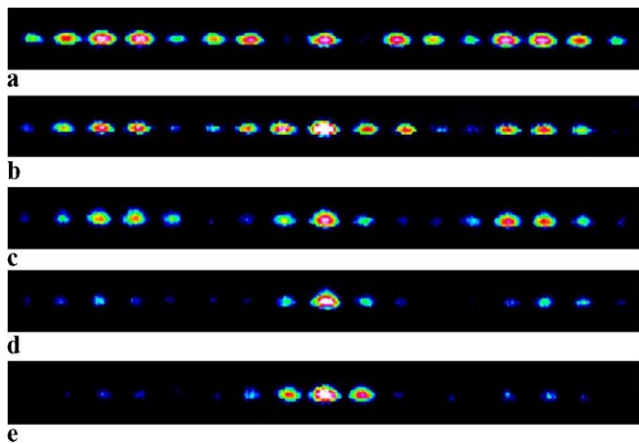
Fig. 2 Light propagation in defect structures recorded with different velocities $v = 30$ (**b**), 20 (**c**), 10 (**d**), and 4 μm/s (**e**) of the focused light spot and fixed optical power $P = 5.5$ mW. For comparison discrete diffraction in a defect-free sample (**a**) is shown, too

(see Fig. 1(b)), while the recording power P is fixed. Different examples of light propagation in such defect structures are shown in Fig. 2, where the defect channel has been excited and the output light distribution on the end-facet is monitored. For increasing deposited energy (lower velocity, i.e., decreasing effective index of the channel) discrete diffraction is increasingly suppressed. For a velocity of $v = 10$ μm/s (Fig. 2(d)) the light is guided mostly in the excited (defect) channel, whereas for even higher deposited energy ($v = 4$ μm/s, Fig. 2(e)) intensity starts to broaden again, and light is guided now in the neighboring channels, too. The latter may be attributed to saturation of the recorded refractive index structures, which increases the width of the defect to more than a single channel.

Wave propagation in a lattice containing a single defect can be modeled by solving (1) numerically using a beam propagation method (BPM). For this we use a periodic index profile $\Delta n(x) = 0.011 \cos^2(\pi x/\Lambda)$ describing our WA and a Gaussian-like defect structure $\delta n(x) = -\delta n_{nl} \exp(-(x - x_0)^2/\sigma^2)$ of the channel located at position x_0. Here $\sigma = 2.1$ μm is the width (Gaussian beam radius) of the defect. In Fig. 3, the calculated output intensity profiles for a propagation length of $L = 17.5$ mm for different defect structures are given. By varying the nonlinear refractive index change δn_{nl} as the only free parameter, a fairly good agreement between experiment and modeling can be obtained. When comparing experiment and numerical modeling we find that an index amplitude of about

Fig. 3 Numerical BPM results for light propagation in a WA containing single defects. Refractive index changes (defect strengths) are $\delta n_{nl} = 0$ (**a**), $\delta n_{nl} = 0.5 \times 10^{-4}$ (**b**), 1×10^{-4} (**c**), and 3.5×10^{-4} (**d**)
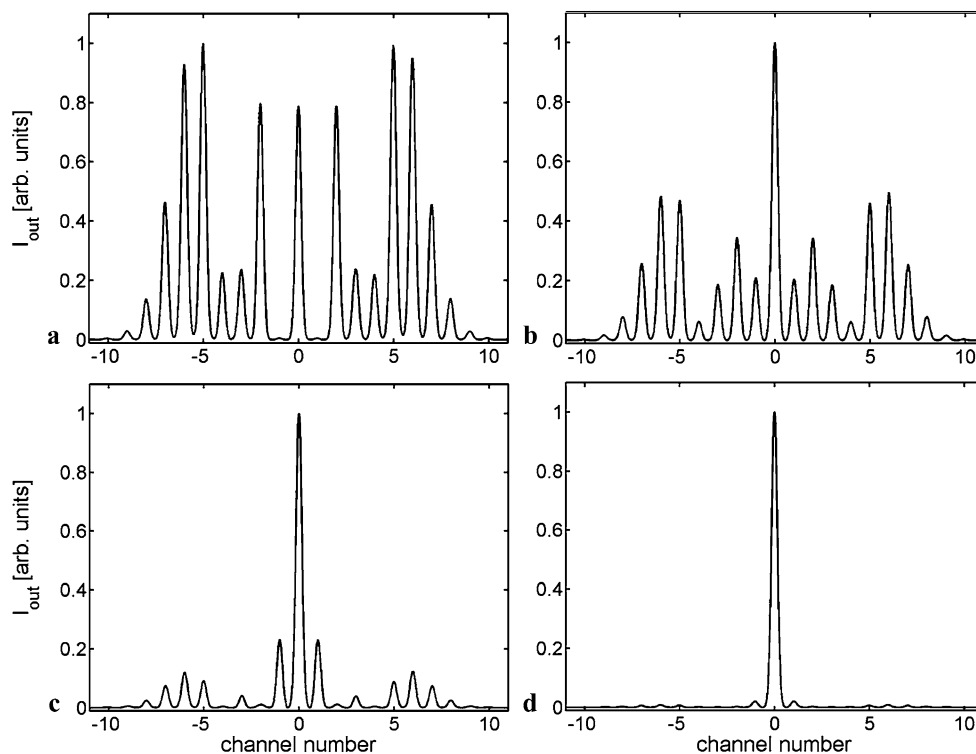
3×10^{-4} results in a defect structure with only weak leakage to neighboring channels.

3.2 Two-channel directional couplers

The possibility to transfer light power from one channel waveguide to another is a key function for numerous applications in miniaturized optical components. For this purpose, directional couplers may be used, which rely on the extension of the evanescent electric field outside the guiding core region. If the evanescent fields of two waveguides overlap, light power can be coupled between the two interacting modes. Here this function may be achieved by recording two adjacent defects in the WA. In Fig. 4, the guiding properties of such a light-induced two-channel directional coupler are given. As can be seen, most of the light coupled into one of the two channels on the input facet is guided/coupled among the two channels.

On the other hand, a smaller part of the light power also leaks out of the structure, which may be due to a too small index decrease of the recorded defects. This explanation is in agreement with results obtained from BPM modeling of the coupler structure in Fig. 4(b), where similar leakage effects are found for a refractive index amplitude of $\delta n_{nl} = 3 \times 10^{-4}$. In numerics, if the index amplitude is further increased, leakage of light out of the two channels is largely suppressed. By varying the length of the coupler structure, any desired splitting ratio of the guided light can be obtained easily.
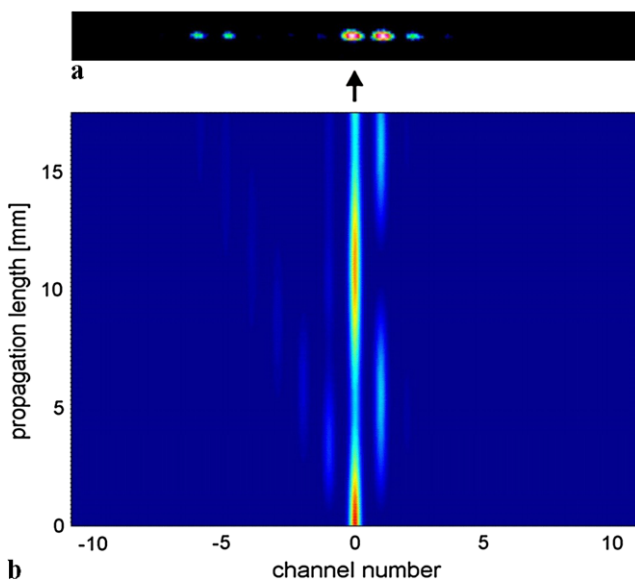
Fig. 4 (**a**) Experimental realization of a two-channel directional coupler in a 1D WA. Shown is the output intensity on the endfacet when one of the two channels is excited on the input side. The *small arrow* points to the excited input channel. (**b**) Numerical BPM simulation of the two channel directional coupler with refractive index amplitude $\delta n_0 = 3 \times 10^{-4}$

3.3 Anderson localization in disordered lattices

Based on the results obtained in the former two subsections on formation of single/double defects, we now proceed in fabrication of disordered lattices in order to investigate wave propagation in these samples. In his works on localization effects, Anderson (and his co-workers) has described energy (wave) transport in such disordered potentials by incorporating interference effects among multiple scattering events [24, 25]. As a consequence he was able to predict significant changes in the eigenmodes when a two-dimensional (2D) lattice is locally excited. Beside the expected diffusive behavior of the wave function, which results in complete delocalization of energy covering the whole crystal (thermal equilibrium), for sufficiently strong disorder also energy localization may occur. In this case, the wave function remains concentrated around the local excitation, and an initially conducting material (without disorder) may become insulating. However, due to the strong implications of the model of distortions to be stationary in time, Anderson localization has never been proven directly in solid-state physics without doubt.

It has been shown that the idea of localization is general to many physical systems, including propagation of light in disordered media [26]. One of the concepts discussed for the study of light wave localization is the so-called transverse localization, i.e., an optical system that does not change along the propagation direction but shows disorder in one (or two) transverse dimension(s). In such a configuration, longitudinal uniformity takes over the role of a stationary disordered potential, and recently the group of Segev was able to directly observe wave localization in a 2D system [27]. Shortly thereafter Anderson-like light localization was also realized in a 1D WA fabricated in AlGaAs with permanent random variations of the channel separations [28]. Information of such a statistical finite system is obtained by measuring average quantities; in our case of a 1D WA this is the output intensity spectrum averaged over many differ-
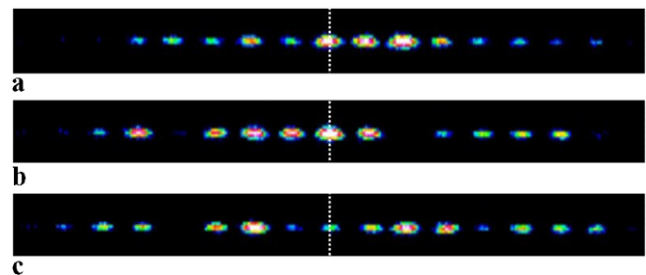
Fig. 5 Experimental examples of intensity diffraction patterns on the output facet in samples with randomly distributed disorder (**a**–**c**) when a single input channel (*dotted line*) is excited. As in these examples propagation dynamics is obviously a statistical process, ensemble-averaged intensity spectra (see Fig. 6) are obtained by averaging over 30 realizations for the same disorder parameters

ent statistical realizations using the same disorder parameters [27]. For zero disorder (a perfect periodic lattice) and local excitation, ballistic wave propagation (linear increase of beam width with propagation distance) will lead to discrete diffraction, i.e., the same output distribution as shown in Figs. 2(a) and 3(a), independent of the respective channel excited on the input side. When disorder increases, the system looses its symmetry, and intensity is now transported randomly in the lattice. However, even for small level of disorder localization effects are expected to occur: In contrast to a (slightly) disordered 2D medium, in a 1D Anderson-like model saturation of wave packets starts immediately, thus no intermediate diffusive regime may be observed. On the other hand, when disorder is sufficiently strong, transmitted energy becomes strongly localized with an exponentially-decaying intensity centered on the initial excitation, analogue to the situation in 2D [27].

Experimentally disordered WA are obtained by varying both, the recording light power in the range [0, P_{max}], and the distance between two recorded straight lines in the range [7 μm, 21 μm], both in a random way (for the latter this means that recorded defects/lines will usually not coincide with the position of permanent waveguide channels). The average strength δn_0 of the disorder is adjusted by using different scan velocities of the moving light focus (along z-direction). In this way, we have fabricated several distorted lattices consisting of 50 waveguide channels, having different level of disorder. We then measured the intensity output distribution for local narrow excitation of the lattice; some examples of asymmetric discrete diffraction in such disordered potentials are given in Fig. 5. For each recorded disordered lattice we average the output intensity spectra over 30 realizations of the same disorder by exciting successively the 30 central channels of the WA (with a total of 50 disordered channels) separately. In Fig. 6, the results of the normalized averaged intensity spectra are plotted for four different settings (zero, small, medium, and strong disorder) as a function of waveguide channel number, relative to the one being excited. For small disorder (scan velocity $v = 80$ μm/s) in Fig. 6(b), only small deviations from the purely ballistic transport (i.e., the case of discrete diffraction in Fig. 6(a)), accompanied with a growth of the central peak monitoring the build-up of a localized component, are observed. When the velocity is halved to $v = 40$ μm/s and thus disorder increased in Fig. 6(c), the central peak grows further, while ballistic transport of energy is merely suppressed.

Fig. 6 Experiment: Averaged output light intensity distribution $\langle I \rangle$ for local excitation of randomly disordered 1D WA for (**a**) zero disorder; (**b**) small disorder, scan velocity $v = 80$ μm/s; (**c**) medium disorder, $v = 40$ μm/s; and (**d**) strong disorder, $v = 20$ μm/s. In (**e**) and (**f**), data from (**c**) and (**d**) is plotted in half-logarithmic scale. The dotted lines show linear fits to the experimental data
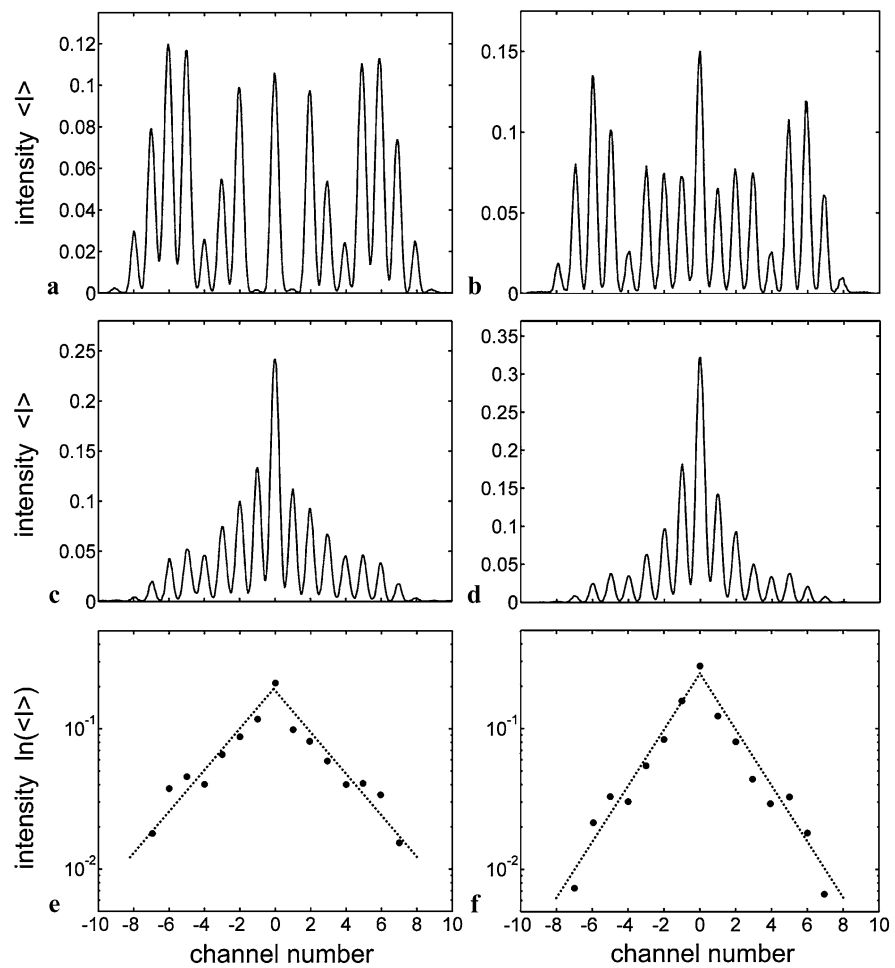
Fig. 7 Simulation: Averaged output intensity distribution $\langle I \rangle$ for local excitation of randomly disordered 1D WA with refractive index amplitude (**a**) $\delta n_0 = 0$; (**b**) $\delta n_0 = 0.5 \times 10^{-4}$; (**c**) $\delta n_0 = 1.25 \times 10^{-4}$; and (**d**) $\delta n_0 = 3.5 \times 10^{-4}$. In (**e**) and (**f**), data from (**c**) and (**d**) is plotted in half-logarithmic scale
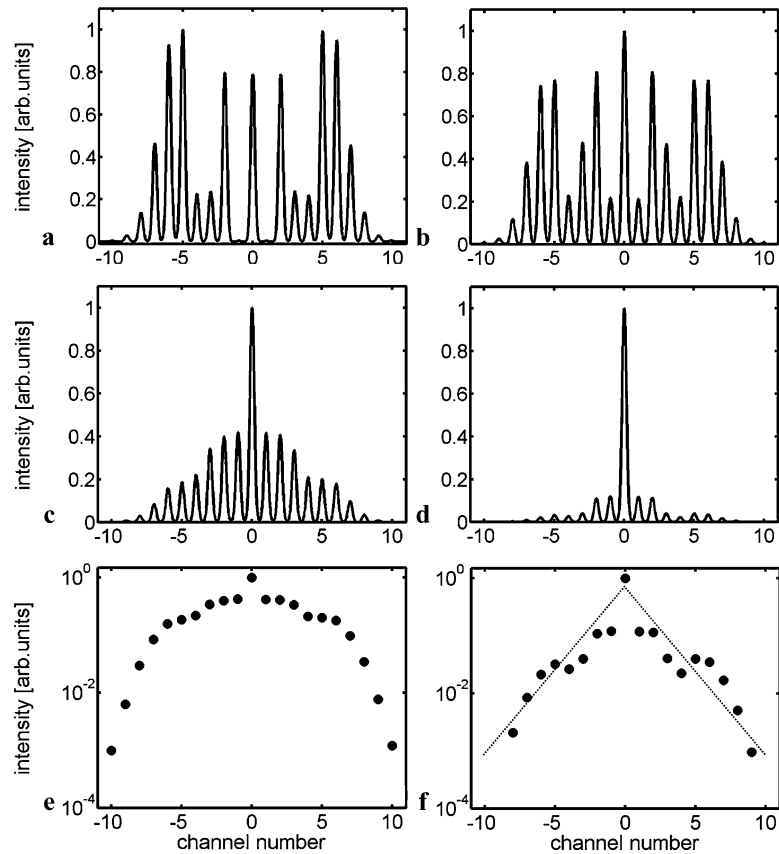
When disorder is further increased ($v = 20\,\mu\text{m/s}$), the output intensity profile narrows further. Now the strong localization regime is reached and broadening of averaged intensity is arrested, see Fig. 6(d). The exponentially decaying tails of the intensity spectrum can be clearly observed in half-logarithmic scale in Fig. 6(e, f), highlighted by linear fits to the data points. Note that the steepness (derivative) of the (linear) fit has increased from (e) to (f), monitoring stronger localization for the latter case.

As before, our disordered system may be again described by the Helmholtz equation (1), with now $\delta n(x)$ being a randomly varying function of transverse direction x, where both periodicity and amplitude are fluctuating. To model the observed localization effects numerically, we perform BPM simulations of light propagation for localized excitations in an array with random distribution of defects. In order to represent the experimental conditions both defect strength (described by a maximum index amplitude δn_0) and local position of defects (in the range (7–21) μm, related to the experimental condition) are varied in a random fashion. Then different input channels (total number are 30 channels) of the disordered lattice are excited, and the corresponding output intensity profiles are averaged and normalized to one for 50 different realizations of a randomly disordered lattice with the same statistical disorder parameters. The results of this procedure are displayed in Fig. 7 for different disorder

strength δn_0. As can be seen, when using reasonable values of the induced random defects strengths, we are able to reproduce the experimental results fairly well. In the experiment, a rather fast transition from ballistic wave transport (Fig. 6(a, b)) to packet saturation (Fig. 6(c)) is observed, which happens for a reduction of the scan velocity of the focused spot by a factor of 2 only (from 80 to 40 μm/s). From the numerically results obtained for recording of both single defects and disordered lattices (for example, Fig. 7(b, c), where part (c) shows such an intermediate situation in simulation), it becomes clear that this range of scan velocities belongs to the case of moderate strength of nonlinear index changes. Here index changes still grow almost exponentially [23], which makes it difficult to adjust intermediate cases of wave transport in disordered lattices experimentally by adjusting the proper scan velocity.

4 Conclusions

In this work, we have studied the influence of light-induced defects on wave propagating in a 1D photonic lattice fabricated in $LiNbO_3$. With the help of a focused light spot that is scanned along one or multiple waveguide channels, we induce negative photorefractive refractive index changes (line defects). For single isolated defects with different strength

we investigate the light guiding properties, and by comparing the experimental results with numerical modeling we find that single channel guidance is obtained for index changes of about $\Delta n_0 \approx 3 \times 10^{-4}$. For the same amplitude of the nonlinearity, also directional couplers may be fabricated in the lattice. Finally, we apply these results to fabricate disordered lattices, having both random variations of defect strength and defect position. In such a system, we observe a transition starting from ballistic energy transport, via an intermediate regime of partially localized components, to Anderson-like light localization for strong disorder.

References

1. J.W. Fleischer, G. Bartal, O. Cohen, T. Schwartz, O. Manela, B. Freedman, M. Segev, H. Buljan, N.K. Efremidis, Opt. Express **13**, 1780 (2005)
2. D.N. Neshev, A.A. Sukhorukov, W. Królikowski, Yu.S. Kivshar, J. Nonlinear Opt. Phys. Mater. **16**, 1 (2007)
3. D.N. Christodoulides, R.I. Joseph, Opt. Lett. **13**, 794 (1988)
4. J.W. Fleischer, M. Segev, N.K. Efremidis, D.N. Christodoulides, Nature **422**, 147 (2003)
5. F. Chen, M. Stepić, C.E. Rüter, D. Runde, D. Kip, V. Shandarov, O. Manela, M. Segev, Opt. Express **13**, 4314 (2005)
6. D. Mandelik, H.S. Eisenberg, Y. Silberberg, R. Morandotti, J.S. Aitchison, Phys. Rev. Lett. **90**, 53902 (2003)
7. C.E. Rüter, J. Wisniewski, D. Kip, Opt. Lett. **31**, 2768 (2006)
8. H.S. Eisenberg, Y. Silberberg, R. Morandotti, J.S. Aitchison, Phys. Rev. Lett. **85**, 1863 (2000)
9. T. Pertsch, P. Dannberg, W. Elflein, A. Brauer, F. Lederer, Phys. Rev. Lett. **83**, 4752 (1999)
10. H.S. Eisenberg, Y. Silberberg, R. Morandotti, A.R. Boyd, J.S. Aitchison, Phys. Rev. Lett. **81**, 3383 (1998)
11. A. Maluckov, M. Stepić, D. Kip, L. Hadzievski, Eur. Phys. J. B **45**, 539 (2005)
12. M. Stepić, C. Wirth, C.E. Rüter, D. Kip, Opt. Lett. **31**, 247 (2006)
13. C.E. Rüter, J. Wisniewski, D. Kip, Opt. Express **15**, 6320 (2007)
14. D. Neshev, A.A. Sukhorukov, B. Hanna, W. Krolikowski, Y.S. Kivshar, Phys. Rev. Lett. **93**, 083905 (2004)
15. D. Mandelik, R. Morandotti, J.S. Aitchison, Y. Silberberg, Phys. Rev. Lett. **92**, 93904 (2004)
16. P.V. Braun, S.A. Rinne, F. Garcia-Santamaria, Adv. Mater. **18**, 2665 (2006)
17. S.A. Rinne, F. Garcia-Santamaria, P.V. Braun, Nat. Photon. **2**, 52 (2008)
18. L. Pang, W. Nakagawa, Y. Fainman, Appl. Opt. **42**, 5450 (2003)
19. J. Scrimgeour, D.N. Sharp, C.F. Blanford, O.M. Roche, R.G. Denning, A.J. Turberfield, Adv. Mater. **18**, 1557 (2006)
20. J. Meier, G.I. Stegeman, D.N. Christodoulides, Y. Silberberg, H. Yang, G. Salamo, M. Sorel, J.S. Aitchison, Opt. Lett. **30**, 1027 (2005)
21. E. Smirnov, C.E. Rüter, M. Stepic, V. Shandarov, D. Kip, Opt. Express **14**, 11248 (2006)
22. M. Stepić, E. Smirnov, C.E. Rüter, L. Prönneke, D. Kip, V. Shandarov, Phys. Rev. E **74**, 046614 (2006)
23. C.E. Rüter, D. Kip, Phys. Rev. A **77**, 013818 (2008)
24. P.W. Anderson, Phys. Rev. **109**, 1492 (1958)
25. E. Abrahams, P.W. Anderson, D.C. Licciardello, T.V. Ramakrishnan, Phys. Rev. Lett. **42**, 673 (1979)
26. S. John, Phys. Rev. Lett. **53**, 2169 (1984)
27. T. Schwartz, G. Bartal, S. Fishman, M. Segev, Nature **446**, 52 (2007)
28. Y. Lahini, A. Avidan, F. Pozzi, M. Sorel, R. Morandotti, D.N. Christodoulides, Y. Silberberg, Phys. Rev. Lett. **100**, 013906 (2008)